The oxygen reduction reaction on palladium with low metal loadings: the effects of chlorides on the stability and activity towards hydrogen peroxide

Guilherme V. Fortunato[a,b,c], Enrico Pizzutilo[b], Eduardo S. F. Cardoso[a], Marcos R. V. Lanza[c], Ioannis Katsounaros[d], Simon J. Freakley[e], Karl J. J. Mayrhofer[b,d,f], Gilberto Maia[a] and Marc Ledendecker[b,g*]*

[a]Institute of Chemistry, Universidade Federal de Mato Grosso do Sul; Av. Senador Filinto Muller, 1555; Campo Grande, MS 79074-460, Brazil

[b]Department of Interface Chemistry and Surface Engineering, Max-Planck-Institut für Eisenforschung GmbH, Max-Planck-Straße 1, 40237 Düsseldorf, Germany

[c]Institute of Chemistry of São Carlos, Universidade de São Paulo, Avenida Trabalhador São-Carlense 400, São Carlos, SP 13566-590, Brazil

[d]Forschungszentrum Jülich, Helmholtz-Institute Erlangen-Nürnberg for Renewable Energy (IEK-11), Egerlandstr. 3, 91058 Erlangen, Germany

[e]Department of Chemistry, University of Bath, Claverton Down, Bath BA2 7AY, UK

[f]Department of Chemical and Biological Engineering, Friedrich-Alexander-Universität Erlangen-Nürnberg, Egerlandstr. 3, 91058 Erlangen, Germany

[g]Department of Technical Chemistry, Technical University Darmstadt, Alarich-Weiss-Straße 8, 64287 Darmstadt, Germany

ABSTRACT: Hydrogen peroxide is considered one of the most important commodity chemicals worldwide but its main production method, the anthraquinone process, poses serious logistical, environmental and safety challenges. Electrocatalytic synthesis through the reduction of molecular oxygen is a promising H_2O_2 production route. However, the reduction of molecular oxygen is kinetically hindered and stable electrocatalysts with a high activity and selectivity towards the 2-electron transfer reaction are needed. In this work, we evaluated the influence of chloride on catalysts with low palladium loadings on the ORR selectivity towards H_2O_2. We report the factors and dynamics that influence H_2O_2 production and highlight synthesis strategies to obtain close to 100% selectivity. By probing the electrode surface after various degradation cycles, we evaluate the role of adsorbing species and the catalysts oxidation states on the hydrogen peroxide selectivity. We systematically modified the catalyst synthesis using different Pd-precursors that were reduced and supported on high surface area graphene nanoribbons. Identical location transmission electron microscopy was used to probe catalyst dynamics during reaction and the activities and selectivities were measured by a rotating ring disk electrode. We probe the potential boundary conditions that lead to catalyst degradation during accelerated stress tests and potentiostatic polarisation and demonstrate how the catalytically active surface can be revived after degradation. The obtained insights can be used as guideline for the development of active, selective and stable catalysts with low noble metal loadings.

KEYWORDS: oxygen reduction reaction, hydrogen peroxide, palladium, carbon-supported electrocatalyst, stability, chlorides.

1. Introduction

Hydrogen peroxide (H_2O_2) plays a crucial role in industrial, commercial and domestic applications such as waste water treatment, bleaching or as an oxidant in chemical synthesis [1–5]. Currently, around 95% of all H_2O_2 is produced on a large scale in centralized reactors through the anthraquinone process [1–6]. This multistep process requires significant energy input, a well-developed infrastructure and poses substantial challenges in handling of concentrated chemicals with negative effects on the overall sustainability [4,5]. Despite the need of dilute concentrations (usually below 9wt%) for small-scale applications such as water treatment and as antimicrobial agent, hydrogen peroxide is commonly concentrated up to 70 wt% using energy-intensive distillations in order to minimize transport costs [4,5]. The drawbacks of the anthraquinone process are driving development of alternative synthesis approaches such as the heterogeneous direct synthesis or the electrochemical synthesis. In the latter, H_2O_2 is synthesized electrochemically through the 2-electron oxygen reduction reaction (ORR-2e^-) [4,5,7–9]. The synthesis is carried out in a decentralized manner and is considered environmentally friendly since undesirable by-products are not obtained [4,5]. Fuel cells can be operated locally under ambient conditions with high flexibility which has advantages over large scale production sites [8–13]. However, the reduction of molecular oxygen (O_2) is kinetically hindered and stable electrocatalysts with a high activity and selectivity towards the 2-electron transfer reaction are needed [1,7,18–20,8,9,12–17]. While platinum (Pt) and palladium (Pd) with extended surface sites are highly selective towards the full 4e- reduction to water (ORR-4e^-) in weakly adsorbing electrolytes, the addition of halides or sulfates has been found to be beneficial to increase the H_2O_2 selectivity [21–27]. Damjanovic et. al. [21] observed that H_2O_2 can be formed as an intermediate during the ORR on bulk Pt when residual

impurities, possibly of organic nature, are adsorbed on the catalyst surface. Similarly, Markovic et. al. [22] observed increased H_2O_2 formation on Pt(111) surfaces in the presence of bromides. It was proposed that strongly surface adsorbed Br^- can lead to the suppression of O_2 adsorption while adjacent Pt sites are essential for O–O bond splitting, implying that in the presence of Br^- anions, the ORR does not proceed entirely through a 4e- reduction pathway [22]. Schmidt et al. [23] evaluated the changes of both, the activity and the reaction pathway of the ORR on carbon supported Pt catalyst when different anions were present. They observed that trace amounts of chlorides (~ 10^{-4} M Cl^-) lead to a reduced ORR-4e^- and enhanced ORR-2e^- selectivity. In all cases, the focus was laid on Pt and large, extended surfaces and H_2O_2 selectivities below 20% were obtained [23]. Despite the large interest in structure-performance descriptors for the electrocatalytic production of H_2O_2, the role of halides on the electrocatalytic activity, stability and selectivity remains still underexplored, especially for low metal loadings [28–31].

In this work, we evaluate the influence of chlorides and carbonaceous species at low metal-loadings (< 2 wt%) on the oxygen reduction reaction. By probing the electrode surface by X-ray photoelectron spectroscopy (XPS) prior to and after electrocatalysis, we highlight the role of adsorbing species. We methodically modified the synthesis parameters using different Pd-precursors that were reduced and supported on high surface area graphene nanoribbons (Pd/GNR). GNR was used as support since it offers a high amount of oxygen and nitrogen groups to increase interactions and dispersion of supported nanoparticles [32]. We used large interparticle distances of ~200 nm to minimize the effect of H_2O_2 re-adsorption and reduction on neighbouring particles after H_2O_2 formation. Identical location transmission electron microscopy (IL-TEM) was used to probe the catalyst dynamics during reaction and the

activities and selectivities were measured by a rotating ring disk electrode (RRDE). We probe the potential boundary conditions that lead to catalyst degradation during accelerated stress tests and potentiostatic polarisation and demonstrate how the catalytically active surface can be revived after degradation. The acquired insights can be used as guidelines for the development of active, selective and stable catalysts with low noble metal loadings.

2. Experimental section

Reagents and instruments

The chemical compounds utilized were palladium (II) chloride–$PdCl_2$ (≥99.9%, Sigma-Aldrich®, Saint Louis, MO, USA), palladium (II) acetylacetonate–$Pd(C_5H_7O_2)_2$ (≥99.98, Fluka®, Steinheim, Germany), ascorbic acid–$C_6H_8O_6$ (≥99.7%, Supelco®, Laramie, WY, USA), potassium persulfate–$K_2S_2O_8$ (99%, Vetec®, Duque de Caxias, RJ, Brazil), hydrogen peroxide–H_2O_2 (30%, Vetec®, Duque de Caxias, RJ, Brazil), sulfuric acid–H_2SO_4 (98%, Vetec®, Duque de Caxias, RJ, Brazil), phosphorus pentoxide–P_2O_5 (99%, Vetec®, Duque de Caxias, RJ, Brazil), ammonia hydroxide solution (28% in water, Vetec®, Duque de Caxias, RJ, Brazil), sodium nitrate–$NaNO_3$ (99%, Vetec®, Duque de Caxias, RJ, Brazil), hydrochloric acid–HCl (37%, Merck®, Darmstadt, Germany), potassium chloride–KCl (≥99%, Merck®, Darmstadt, Germany), and perchloric acid–$HClO_4$ (70%, Chloride ≤ 0.001%, Merck®, Darmstadt, Germany), potassium permanganate–$KMnO_4$ (98%, Nuclear®, Diadema, SP, Brazil), hydrazine sulfate (99%, Dinâmica®, Diadema, SP, Brazil), and multiwall carbon nanotubes (≥98%, Aldrich®, Saint Louis, MO, USA) with outside diameter of 10 ± 1 nm x internal diameter of 4.5 ± 0.5 nm and 3–6 μm-long with 6–8 tube walls.

All electrochemical measurements were performed in a three-electrode Teflon cell with a rotating ring-disk electrode (RRDE) consisting of Teflon-embedded GC disk/Pt ring assembly with

geometric areas of 0.196 and 0.11 cm^2, respectively. The collection efficiency for the ring electrode (*N)* was 0.26. Separated by a Nafion® membrane, a graphite rod and a saturated Ag/AgCl electrode (Metrohm) served as the counter electrode and reference electrode, respectively. All potentials are plotted against the reversible hydrogen electrode (RHE) potential. Before every measurement, its potential vs. an Ag/AgCl electrode was measured in the corresponding electrolyte after hydrogen saturation.

Materials characterization

For IL-TEM and TEM experiments, the catalyst dispersion was drop casted onto a TEM grid constituted of a lacey carbon film supported by a 400-mesh gold grid. The identical location of the catalysts before and after the accelerated stress test (AST-1.0) was examined by TEM utilizing a JEOL JEM 2200FS microscope operating at 200 kV.

ICP-MS (NexION 300X, Perkin Elmer) was used to determine the Pd loadings. Before each ICP-MS measurement, the graphene support was removed by heating the catalyst powder in porcelain crucibles at 650 °C in air. The Pd oxide residues were dissolved by boiling in quartz beakers in aqua regia (20 mL) for 45 min followed by the transfer into 100 mL volumetric flasks.

For XPS experiments after electrochemical measurement, the catalyst film placed on a GC plate (used as electrode) was carefully washed several times with ultrapure water to remove electrolyte excess, and dried under Ar flux before subjecting it to the XPS chamber. The XPS measurements were performed on a PHI Quantera II Surface Analysis Equipment and an Omicron surface analysis station equipped with a SPHERA hemispherical analyser. The Al Kα line (1486.6 eV) was used as the ionization source operating at 15 kV and 25 W. The spectra were calibrated by the C 1s signal at 284.8 eV.

Electrode preparation and electrochemical measurements

As working electrode, 20 μL of an aqueous catalyst solution (1.5 mg mL^{-1}) was drop casted onto a GC disk to obtain a catalyst loading of 152.7 μg cm^{-2} and dried at room temperature. The modified electrodes were placed in an electrochemical Teflon cell containing a 0.1 M aqueous solution of $HClO_4$, which was subsequently saturated with Ar or O_2 (both with high purity).

Cyclic voltammetry (CV), RRDE measurements and impedance spectroscopy (EIS) were performed on a Gamry Reference 600 potentiostat coupled to an AFMSRCE modulated speed rotator from Pine Research Instrumentation. EIS results were collected within a frequency range of 10 mHz to 100 kHz with a potential amplitude of 10 mV (rms) at 10 points $decade^{-1}$ around 0.9 V_{RHE}. The ohmic drop resistance was corrected for each RRDE curve. The measured ohmic drop in 0.1 M $HClO_4$ was usually around 35 Ω. The H_2O_2 generated during ORR on the disk electrode was monitored by the Pt ring electrode which was kept constant at 1.28 V_{RHE}.

The experimental protocol was performed on the same catalysts deposited onto the RRDE tip. The freshly synthesized materials were tested towards H_2O_2 production (selectivity and activity) in an RRDE setup. Subsequently, the electrode was submitted to 10,000 potential cycles between 0.1 and 1.0 V_{RHE}. After testing, the electrode was removed from the electrolyte, the catalyst subjected to a 0.1 M KCl solution (20 μL) and the electrode was left until the electrolyte dried. After evaporation at room temperature, the modified electrodes were washed with ultrapure water to remove excess KCl. Afterwards, the activity and selectivity were tested another time before and after 10,000 potential cycles. The mass activity and selectivity results are shown in Figure 4.

Synthesis of GNR

GNR were synthesized from multiwall carbon nanotubes as described before [33].

Synthesis of Pd/GNR catalysts

Initially, 16 mg of GNR were dispersed with 0.550 mg of $PdCl_2$ (or 0.946 mg of $Pd(acac)_2$) in 10 mL ultrapure water by ultra-sonication during at least 40 min. Subsequently, the mixture was heated to 100 °C using a hot plate with magnetic stirring. Afterwards, 1 mL of an aqueous ascorbic acid solution (14.5 mg mL^{-1}) was added. After 5 minutes, the heating was stopped and the mixture was stirred for 2 hours. The formed Pd/GNR-Cl (or Pd/GNR-acac) nanocomposite was washed by centrifugation with ultrapure water (10 times) to remove not reacted reactants present in the mixture, and finally dried in an oven at 40 °C.

3. Results and discussion:

In order to obtain first insights how chloride ions influence the ORR at low metal loadings, two sets of catalyst materials have been prepared. Specifically, palladium acetylacetonate ($Pd(acac)_2$) was selected as precursor excluding explicitly surface adsorbing halides while palladium chloride ($PdCl_2$) served as palladium and chloride source. Both precursors were hydrothermally reduced to obtain palladium nanoparticles (Pd/GNR – Cl with $PdCl_2$ as precursor; Pd/GNR-acac with $Pd(acac)_2$ as precursor) in the presence of high surface area graphene nanoribbons as carbon support (Scheme 1). Both precursors resulted in similar surface morphologies and comparable Pd-loadings (0.15 at%), interparticle distances (~200 nm) and particles sizes (~7 nm) as shown in Figure 1 and Table S1 (c.f. Figure S1, Table S2). For both samples, TEM imaging (c.f. Figure 1) suggests that the Pd-NPs are surrounded by not well-defined carbon layers of GNR.

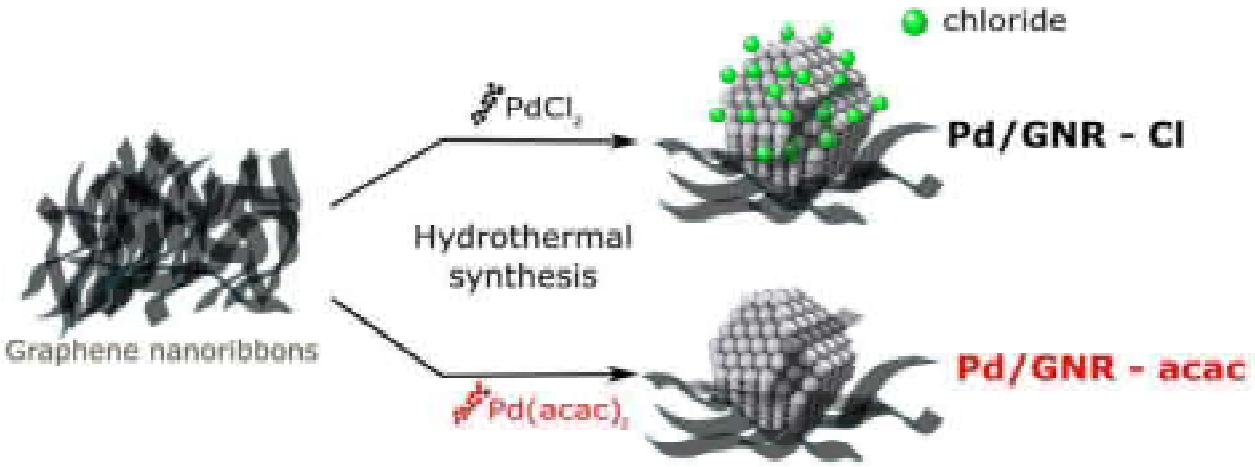

Scheme 1. Schematic representation of the synthesis of supported Pd nanoparticles onto GNR.

The presence and oxidation state of Pd was confirmed by XPS and is shown in Figure 1. For Pd/GNR - Cl, the Cl^- amount was close to the detection limit of the XPS and was estimated to be 0.13 wt% resulting in a Pd/Cl atomic ratio of 3:1. For Pd/GNR - acac, no chloride speciations were detected (Figure S2a). The spectra recorded in the Pd 3d region produced from both precursors exhibit the expected spin-orbit splitting and binding energy of metallic Pd species (Pd $3d_{5/2}$ at ~335 eV, Pd $3d_{3/2}$ at ~340 eV, c.f. Table S3). The doublet at higher binding energies (shifted ~2.7 eV) indicate oxidic Pd speciation which is in accordance with the electron withdrawing nature of adsorbing ligands. Due the low amounts of Pd and Cl, the resolution of the XPS data is low. Taking four different spectra into account, the amount of Pd^0 was found to be slightly higher (~1.6 %) when acetylacetonate was used as precursor while the amount of oxygen remained unchanged (c.f. Tables S2 and S3). The more electron withdrawing nature of Cl^- compared to acac leads to a more oxidized Pd surface - for Pd/GNR-Cl, the Pd $3d_{5/2}$ and Pd $3d_{3/2}$ peaks (Table S3) are shifted on average around 0.3 eV to higher binding energies compared to Pd/GNR-acac —indirectly suggesting an influence of Cl adsorbed onto the Pd/GNR-Cl catalyst surface. The exact local environment and nature of Cl^- can, however, not unambiguously be cleared up.

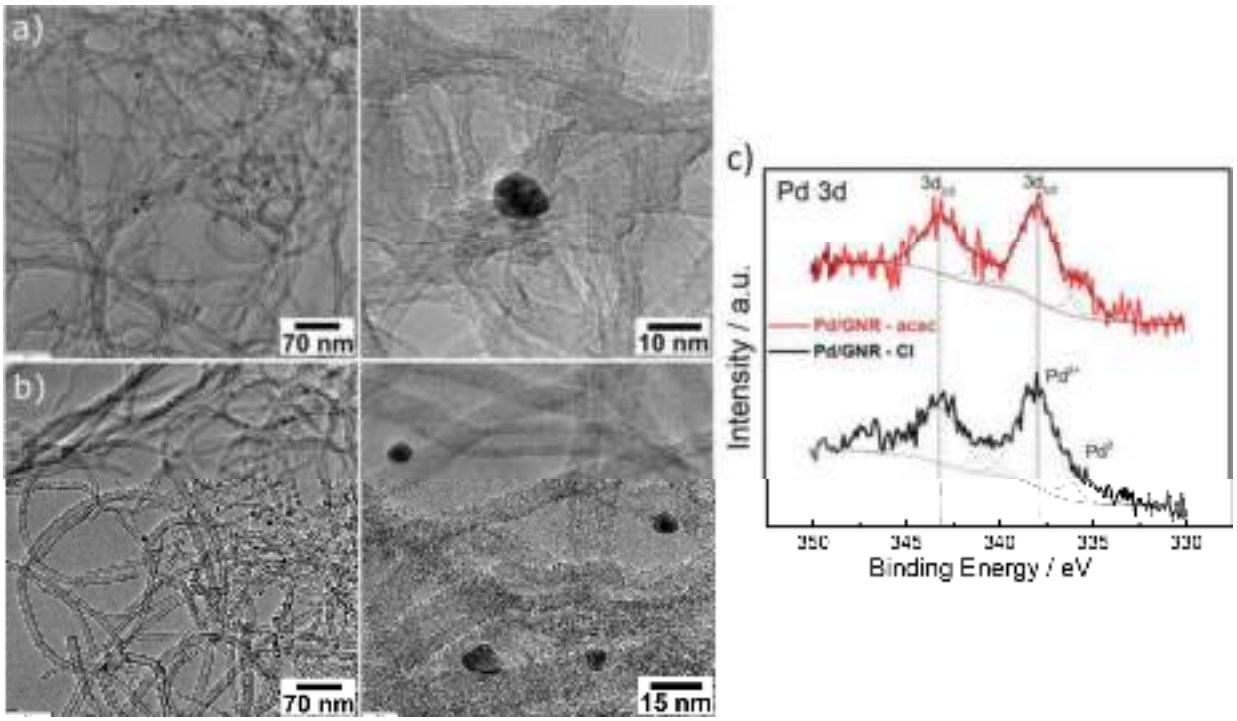

Figure 1. TEM images of (a) Pd/GNR-Cl and (b) Pd/GNR-acac after hydrothermal synthesis. High resolution XPS spectra in the (c) Pd 3d region of Pd/GNR produced from $PdCl_2$ and $Pd(acac)_2$.

Cyclic voltammetry obtained in argon (Ar)-sat. 0.1 M $HClO_4$ between 0.1 V and 1.4 V_{RHE} for both samples are shown in Figure 2. The lower potential limit was selected to be above the hydrogen absorption threshold [34], the upper to include the characteristic redox features of Pd. Both samples exhibit comparable redox features. Due to the low Pd-loading, the characteristic quinone/hydroquinone peaks (at ~0.6 V) from GNR surface functionalities [32,35] prevail. The characteristic adsorption of underpotential deposited hydrogen (H_{UPD}) for bare Pd between 0.1 and 0.4 V_{RHE} [36] was not observed. As no adsorption/desorption charge was measured, the underpotential deposition of hydrogen might be hindered by adsorbed spectator species that occupy similar surface sites as H_{UPD} [37–40]. Studies from Arenz and coworkers suggested that Cl-desorption from Pd between 0.25 and 0.8 V_{RHE} is inhibited leading to a high anion coverage in the potential region of the ORR [26]. It was suggested that with an increase in applied potential, halides adsorption becomes more pronounced competing with oxygen adsorption [41,42]. Similarly, the

Pd oxidation region over ~0.85 V_{RHE} is affected by the low metal loading and the adsorbed spectators, and the characteristic peaks are strongly suppressed for both materials. Additionally, the cyclic voltammogram for bare GNR reveals the oxidation of graphene is comparably small compared to Pd-oxidation and that a possible overlap cannot be detected. When Pd-surface oxidation commences, chemisorbed halide ions were reported to desorb from the surface [43]. Careful inspection of the cyclic voltammogram in the negative scan direction between 0.8 and 0.6 V_{RHE} reveals the characteristic oxide reduction peak which is more pronounced for the chloride-free catalyst. Due to the strong metal-chloride affinity, adsorbed chloride species suppress the characteristic oxide reduction peak which is in line with literature.[22,23] Schmidt et al. observed a decrease in oxide reduction peak charge for a carbon supported Pt catalyst [23] when the chloride concentration was increased.

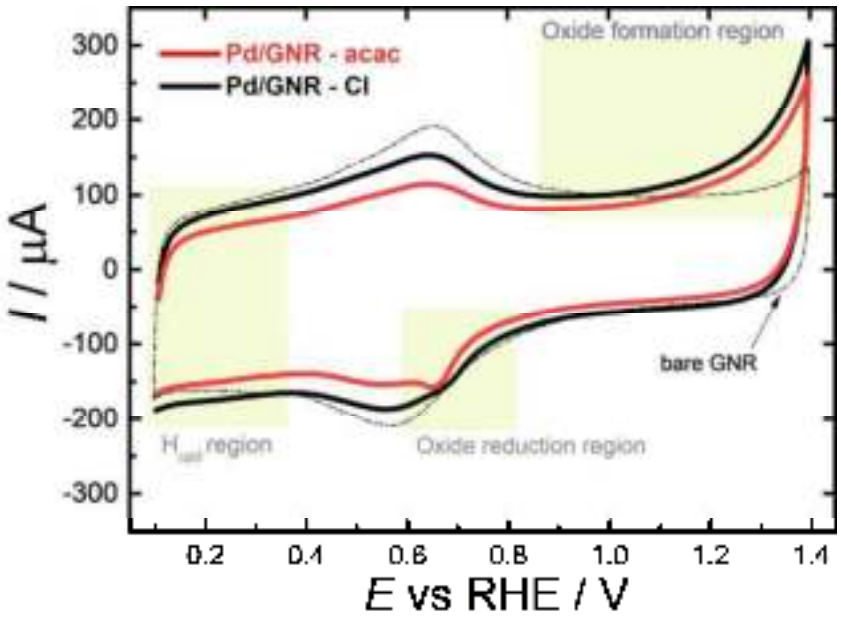

Figure 2. Cyclic voltammograms of Pd/GNR – acac, Pd/GNR – Cl, and bare GNR between 0.1 and 1.4 V_{RHE} in Ar-sat. 0.1 M $HClO_4$ at a scan rate of 50 mV s^{-1}.

In order to determine the activity and selectivity, both samples were tested towards the production of H_2O_2 by scanning the potential from 0.1 to 1.0 V_{RHE} in a rotating ring disk electrode (RRDE) setup in O_2-sat. 0.1 M $HClO_4$ (Figure 3). The rotating ring disk electrode provides information about the potential dependent selectivity towards H_2O_2 (S_{H2O2}) in the course of the ORR. The fraction of H_2O_2 can be calculated from the measured disk current, I_D, the ring currents for H_2O_2 oxidation, I_R, and the collection efficiency of the system, *N*, according to equation 1 [44,45].

$$S_{H_2O_2} = \frac{2I_r/N}{I_d + I_r/N} \; x \; 100\% \qquad (1)$$

For Pd/GNR-acac, S_{H2O2} reaches 60% while for Pd/GNR-Cl, the selectivity reaches 86 % over the measured potential range from 0.1 V to 0.5 V_{RHE}. For both catalysts, high selectivities were obtained while the additional presence of chlorides appear to break the extended Pd-arrangement successfully and the full reduction to H_2O becomes less favorable [46,47].

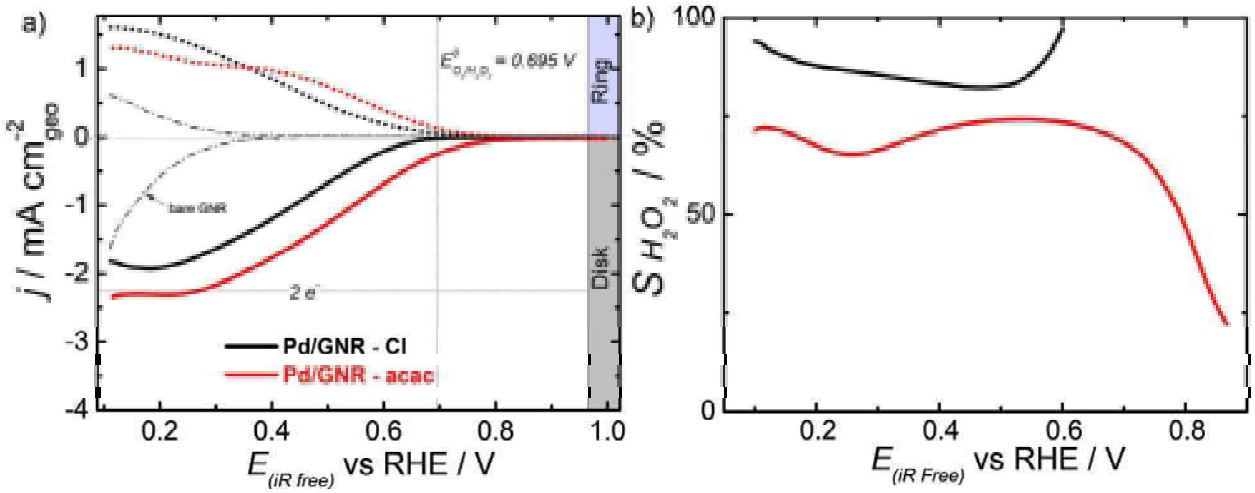

Figure 3. (a) Linear sweep RRDE results for Pd/GNR-Cl and Pd/GNR-acac in O_2-sat. 0.1 M $HClO_4$ at 50 mV s^{-1} and 900 rpm. The potential was swept from 0.1 to 1.0 V_{RHE}. (b) $S_{H_2O_2}$ during the ORR at varying potentials. ´

In order to elaborate on the role of chlorides in both samples, the surface was deliberately modified by adding 20 µL of a 0.1 M aqueous KCl solution and letting the solvent evaporate (denoted as "+ Cl^-"). Cation-palladium interactions have been reported to be much weaker compared to anion-

palladium interactions and are therefore considered to only influence marginally the investigated electrode processes [41]. Stability tests with and without the addition of chlorides were performed by RRDE and by cyclic voltammetry and the results are shown in Figures S3 and S4. Additionally, the mass activities (*MA*) were determined from the ring curves at 0.64 V_{RHE} as described in ref. [32] and are, together with the H_2O_2-selectivities, shown in Figure 4.

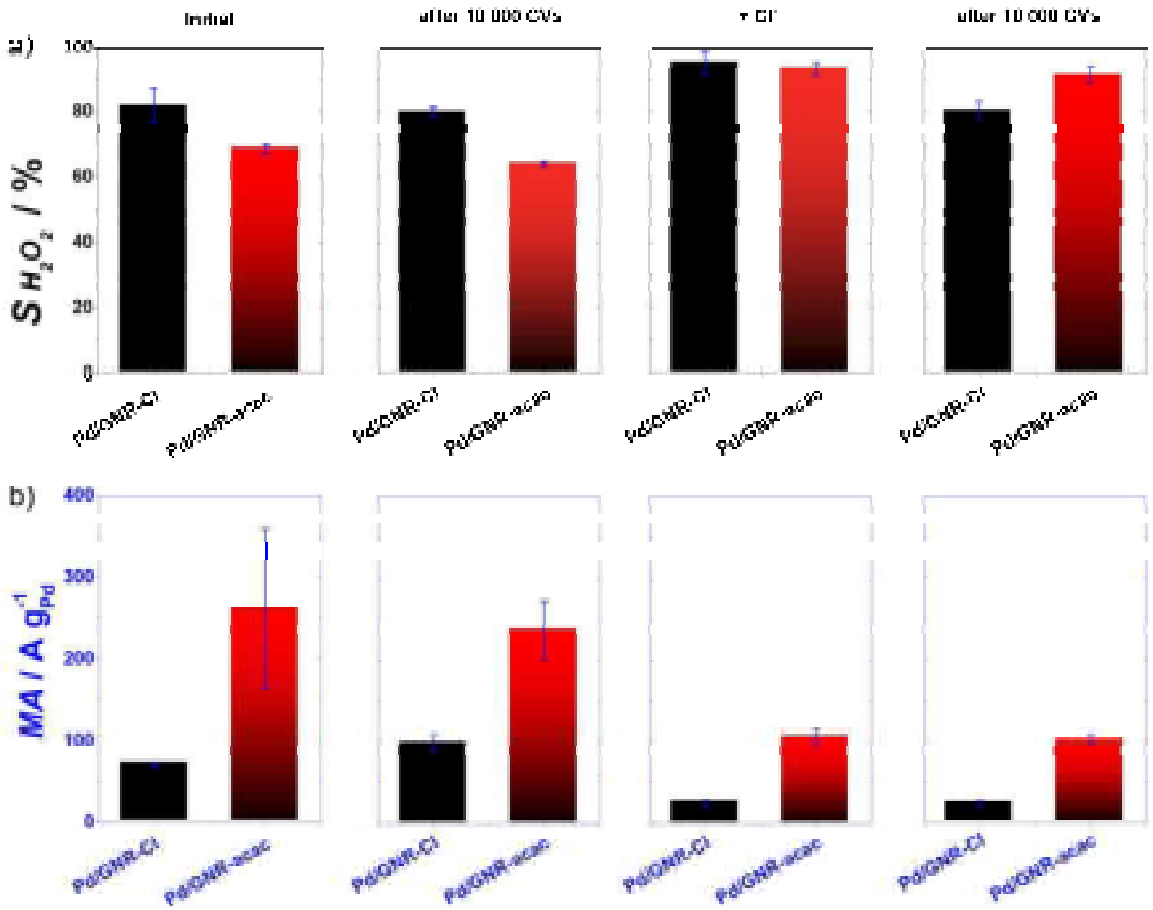

Figure 4. (a) Selectivities of both catalyst systems over a potential range between 0.1 and 0.5 V_{RHE} (initial), after 10,000 degradation cycles between 0.1 and 1.0 V_{RHE}, after adding 20 µL of a 0.1 M aqueous KCl solution and solvent evaporation, after further 10,000 degradation cycles between 0.1 and 1.0 V_{RHE} and (b) the respective *MA* at an overpotential of 50 mV (values were obtained from the ring curves of the RRDE results shown in Figure S4. The error bars represent the confidence intervals (at the 95% confidence level) of at least two measurements.

For Pd/GNR-Cl, the selectivity is practically unchanged ($S_{H_2O_2}$ changes from 84 to 81%) after the accelerated stress test consisting of 10,000 cycles between 0.1 and 1.0 V_{RHE} (AST-1.0) while the

MA for the production of H_2O_2 increases (from 71 to 98 A g^{-1}_{Pd}). The XPS spectra for the Pd 3d and C 1s and O 1s region (Figure S5) suggest that changes such as surface oxidation and adsorbate removal take place after the AST-1.0. A slight shift to higher binding energies and a decrease in Pd^{2+} to Pd^0 ratio (c.f. Figure S5a) suggest the removal of adsorbates and, consequently, a partial reduction of ionic Pd speciation to metallic Pd. The graphene nanoribbons are stable at AST-1.0 and no carbon oxidation is observed in the C 1s spectrum (Figure S5c). In order to test the reversibility of the tested system, the catalyst was re-subjected to 20 µL of a 0.1 M aqueous KCl solution after AST-1.0, the solvent was evaporated and the selectivity and activity were re-measured (Figure 4 and Figure S4). After the addition of Cl^-, the selectivities are drastically increased reaching almost 100%. At the same time, the mass activity decreases. We assigned the changed mass activity to the decrease of available Pd sites and a suppressed formation of Pd surface oxides after Cl^- addition as observed in the voltammograms in Figure S4c. Additionally, as the number of electrons that are exchanged per oxygen molecule decreases, the mass activity decreases. The material is stable during 10,000 degradation cycles and the influence of chlorides on the selectivity and activity remains. Interestingly, the highest selectivities and mass activities are achieved when GNR-acac is modified with Cl^- hinting to an interplay between geometric (site-blocking) and electronic effects (ligand effects) similar to reports in the field of heterogeneous catalysis [48–50].

Subsequently, a method was developed to remove surface chlorides and carbonaceous species by applying a potential of 1.6 V_{RHE}. The challenge lies in removing strongly bound surface adsorbed chlorides while still keeping the carbon support intact. Despite the kinetic stabilization of the carbon support, carbon corrosion at potentials over 1.0 V_{RHE} in acidic electrolyte have been

observed [51–53]. The Cl^--removal efficiency was probed by electrochemical-, spectroscopic- and microscopic analysis.

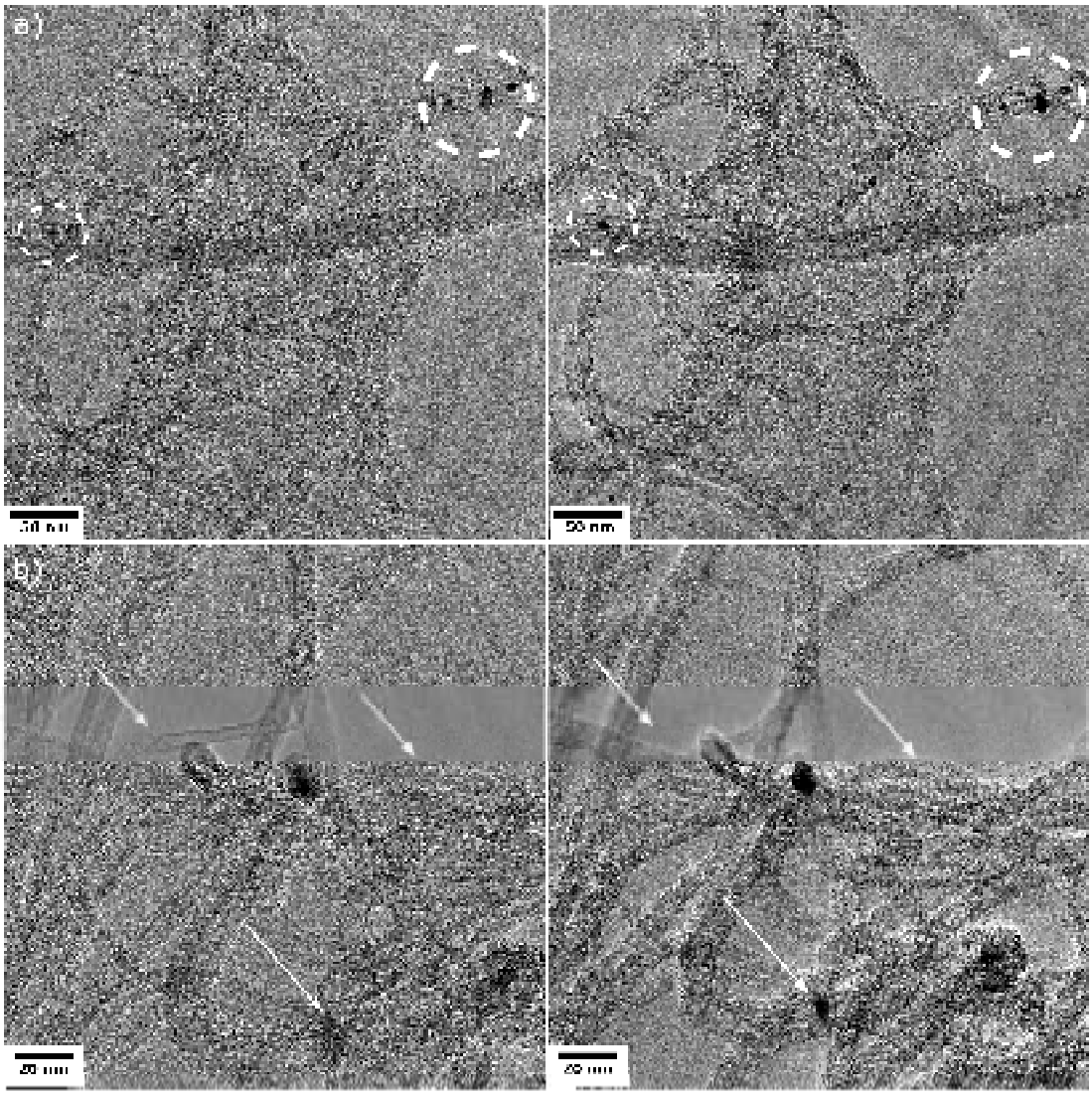

Figure 5. Identical location transmission electron micrographs of two distinct surface regions (a, b) of Pd/GNR-Cl before (left) and after (right) chronoamperometric polarization at 1.6 V_{RHE} for 30 min in 0.1 M $HClO_4$.

Figure S6a shows the chronoamperogram at 1.6 V_{RHE} recorded in 0.1 M $HClO_4$ over a time interval of 30 minutes. By subjecting the catalyst surface to oxidative potentials, various redox-reactions can take place including the oxygen evolution reaction, the oxidation/dissolution of palladium, carbon corrosion and the chlorine evolution reaction (CER). The equilibrium potential of the Cl^-

/Cl_2 couple for the CER on the standard hydrogen electrode (SHE) potential scale is $E = 1.395 + 0.0295 \log([Cl_2]/[Cl^-]^2)$ [54]. Assuming a higher ratio of $[Cl^-]/[Cl_2]$, an additional onset shift to more negative potentials than the standard electrode potential is expected. The XPS spectra in the 3d Pd and 1s C and 1s O regions after chronoamperometry (CA) at 1.6 V_{RHE} for 30 minutes are shown in Figure S7. The minor peak shift in the 3d-Pd region of ca. 0.23 eV to higher binding energies suggests slight oxidation of the Pd surface after chronoamperometry which is expected (red arrow, Figure S7a). In the C 1s region (Figure S7b), an additional peak at 288.7 eV appears, which can be attributed to the presence of oxygenated groups such as C=O and COOH, in line with an increased elemental amount of oxygen (O 1s spectra in Figure S7c) [55,56]. To track structural and morphological changes of individual particles and to identify support modifications, identical location transmission electron microscopy (IL-TEM) was used prior to and after chronoamperometry. After 30 minutes at 1.6 V_{RHE}, the Pd particles slightly reduced in size as shown in Figures 5 presumably due to dissolution of Pd when oxidized [57]. The main particles neither agglomerate nor detach during the cleaning treatment. However, occasional detachment of Pd-clusters was observed. Minor carbon corrosion was observed as indicated in Figure 5 exposing more of the Pd surface. Cl-removal has drastic consequences for the electrochemical H_2O_2 production as shown in Figure S8. After Cl-removal, a decrease in selectivity from 84 to 48% in the potential range between 0.5 and 0.2 V_{RHE} was observed. At the same time, the mass activity increases which can be attributed to a greater exposure of Pd surfaces due to carbon and chloride oxidation. To elaborate further on the time scale at which the surface cleaning takes place, the ring and disk currents were monitored after various chronoamperometric measurement times at 1.6 V_{RHE} as shown in Figure S8. In line with previous results, the fraction of H_2O_2 decreases when the polarisation time is extended. After 10 min, the selectivities remain almost constant hinting to a stabilization of the Pd surface. S_{H2O2} decreases with increasing polarisation time even below the

initial value of 63% at 0.5 V_{RHE}. As chloride desorption was reported in and below the H_{UPD} region (<~0.4 V_{RHE}) as well as when PdO is formed (<~0.85 V_{RHE}) [43], the potential was held exemplarily at -0.2 V_{RHE} and 1.2 V_{RHE} for 5 min and the activity and selectivity was monitored. In both cases, the potential proved to be not sufficient to remove chlorides from the catalyst surface (Figure S9) as similar selectivities were obtained prior to and after chronoamperometry. It also shows that temporary occurring Cl^--desorption is not sufficient to have an impact on the selectivity and (solvated) Cl^- in close vicinity to the surface might re-adsorb during or before ORR testing.

To further investigate the influence of chlorides on the previously cleaned surface, 20 µL of a 0.1 M aqueous KCl solution was added and the solvent was evaporated. The cyclic voltammograms for Pd/GNR-acac in different Cl^- concentrations are shown in Figure S10C. Figure 6 displays the RRDE results after the removal and re-addition of surface chlorides and their impact on the ORR activity and selectivity. When chlorides are deliberately added, the selectivity increases again.

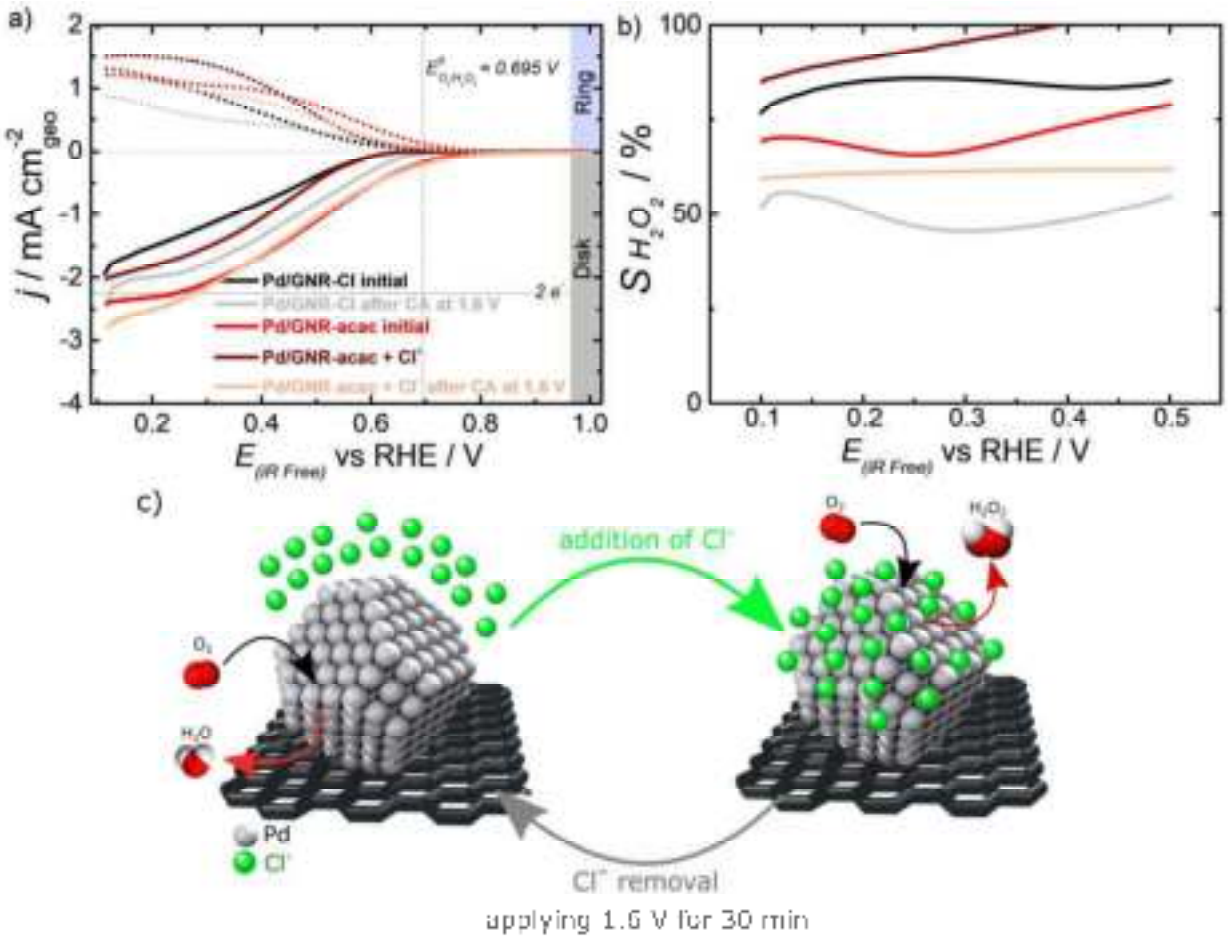

Figure 6. (a) Linear sweep RRDE results scanning the potential at 50 mV s^{-1} from 0.1 to 1.0 V_{RHE} at 900 rpm in O_2-sat. 0.1 M $HClO_4$ in the presence/absence of chlorides. (b) $S_{H_2O_2}$ during the ORR at varying potentials (obtained from the corresponding RRDE data). (c) Schematic showing the influence of chlorides on the catalysts surface, the impact on the selectivity and the suggested treatment for Cl^- removal.

When chlorides are added to Pd/GNR-acac, the selectivities increase from 69 to 93% while the activity decreases as evidenced by the shifted disk and ring curves to lower potentials. The current densities j_d are close to the theoretically expected current density for a 2-electron transfer.

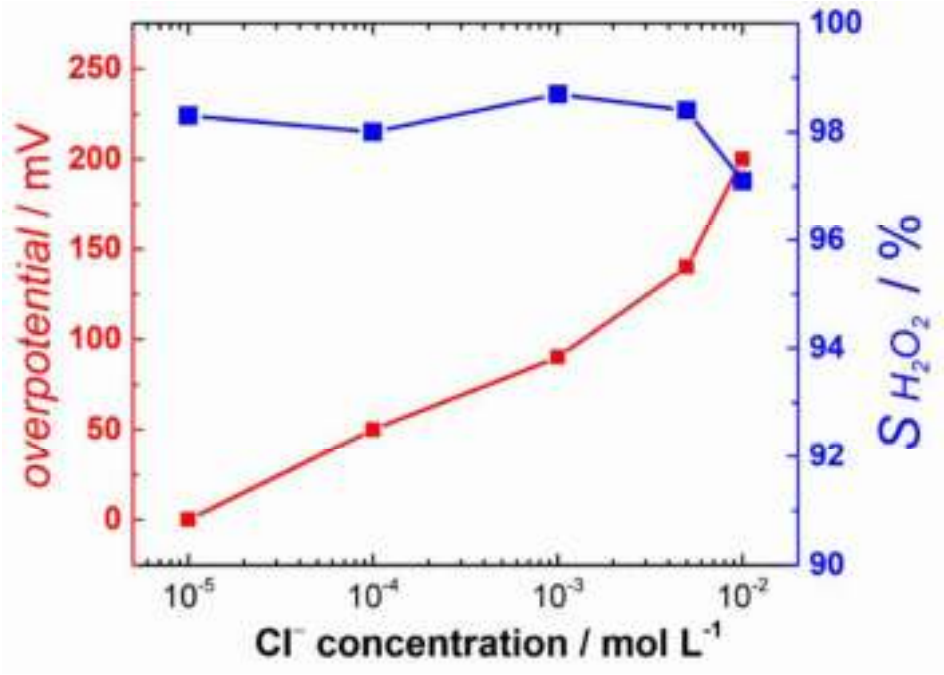

Figure 7. Correlation of overpotential (with respect to the thermodynamically expected standard electrode potential $E^0_{O2/H2O2}$ = 0.695 V_{RHE}) and H_2O_2 selectivity at various chloride concentrations in the electrolyte (values were obtained from RRDE shown in Figure S10 and Table S4). The ring was held at 1.28 V_{RHE}. We note that at high Cl^- concentrations, the determination of H_2O_2 is less precise which we attributed to the decline in selectivity at Cl^- concentration of $5x10^{-2}$ M.

As reference, we monitored the selectivity and activities after adjusting the Cl^- concentration in the electrolyte from 10^{-5} to 10^{-2} M. We observed a linear correlation of chloride adsorption and ORR overpotential while the selectivity remains comparable at over 90% over the measured Cl^- concentration regime (Figure 7 and S10). Additionally, with increasing Cl^- concentration, the palladium oxidation peak becomes supressed suggesting adsorbed chlorides on the Pd-surface. After electrolyte exchange, the Pd-oxidation peak remains supressed confirming the strong metal-chloride interaction.

4. Conclusions

In summary, we have evaluated the influence of chloride on palladium for the oxygen reduction reaction at low metal loadings. The interplay of geometric and electronic effects promotes the

formation of H_2O_2 with selectivities close to 100% with almost no kinetic overpotential while keeping the mass activity high. When Cl^- are adsorbed onto the Pd-surface, the catalyst maintains the propensity for the selective production of H_2O_2 during accelerated stress tests between 0.1 to 1.0 V_{RHE}. Adsorbed surface species can be effectively removed by a proposed electrochemical method polarizing the electrode at 1.6 V_{RHE} for various times. Additionally, we describe the relationship between activity, stability and selectivity of low palladium loadings towards the production of H_2O_2. The obtained insights can be used as guideline for the development of active, selective and stable catalysts with low noble metal loadings.

ASSOCIATED CONTENT

Supporting Information. The supporting information contains figures, equations, and tables concerning supplementary results, and references. This material is available free of charge via the Internet at:

AUTHOR INFORMATION

Corresponding Authors

* Marc Ledendecker: marc.ledendecker@tu-darmstadt.de

* Guilherme V. Fortunato: g.fortunato@usp.br

Author Contributions

The manuscript was written through contributions of all authors. All authors have given approval to the final version of the manuscript.

ACKNOWLEDGMENTS

The authors acknowledge the financial support provided by the Brazilian funding agencies, including the Brazilian National Council for Scientific and Technological Development - CNPq (grants. #303351/2018-7, #405742/2018-5, and #302874/2017-8), São Paulo Research Foundation (FAPESP – grants #2017/10118-0 and #2019/04421-7), and the Coordenação de Aperfeiçoamento de Pessoal de Nível Superior (CAPES – Finance Code 001), CAPES-PRINT (grant #88881.311799/2018-01). E.S.F.C. would also like to extend his gratitude to PNPD-CAPES for the assistance and as G.V.F. thanks CAPES for the PDSE fellowship (grant #88881.131904/2016-01). K.J.J.M. acknowledge the Federal Ministry for Economic Affairs and Energy (BMWi) of Germany in the framework of PtTM@HGS (project number 03ET6080A) for funding. M.L. acknowledge the Federal Ministry of Education and Research (BMBF) in the framework of NanoMatFutur (SynKat) for financial support (project number 03XP0265). The authors thank the LAMAS – Laboratório Multiusuário de Análise de Superfícies from UFRGS for the XPS facilities.

REFERENCES

[1] L. Pesterfield, The 100 Most Important Chemical Compounds: A Reference Guide (by Richard L. Myers), J. Chem. Educ. 86 (2009) 1182. doi:10.1021/ed086p1182.

[2] J.M. Campos-Martin, G. Blanco-Brieva, J.L.G. Fierro, Hydrogen peroxide synthesis: An outlook beyond the anthraquinone process, Angew. Chemie - Int. Ed. 45 (2006) 6962–6984. doi:10.1002/anie.200503779.

[3] J.K. Edwards, S.J. Freakley, R.J. Lewis, J.C. Pritchard, G.J. Hutchings, Advances in the direct synthesis of hydrogen peroxide from hydrogen and oxygen, Catal. Today. 248 (2015) 3–9. doi:10.1016/j.cattod.2014.03.011.

[4] S. Yang, A. Verdaguer-Casadevall, L. Arnarson, L. Silvioli, V. Čolić, R. Frydendal, J. Rossmeisl, I. Chorkendorff, I.E.L. Stephens, Toward the Decentralized Electrochemical

Production of H2O2 : A Focus on the Catalysis, ACS Catal. 8 (2018) 4064–4081. doi:10.1021/acscatal.8b00217.

[5] Y. Jiang, P. Ni, C. Chen, Y. Lu, P. Yang, B. Kong, A. Fisher, X. Wang, Selective Electrochemical H2O2 Production through Two-Electron Oxygen Electrochemistry, Adv. Energy Mater. 8 (2018) 1801909. doi:10.1002/aenm.201801909.

[6] S.C. Perry, D. Pangotra, L. Vieira, L.-I. Csepei, V. Sieber, L. Wang, C. Ponce de León, F.C. Walsh, Electrochemical synthesis of hydrogen peroxide from water and oxygen, Nat. Rev. Chem. (2019). doi:10.1038/s41570-019-0110-6.

[7] E. Pizzutilo, O. Kasian, C.H. Choi, S. Cherevko, G.J. Hutchings, K.J.J. Mayrhofer, S.J. Freakley, Electrocatalytic synthesis of hydrogen peroxide on Au-Pd nanoparticles: From fundamentals to continuous production, Chem. Phys. Lett. 683 (2017) 436–442. doi:10.1016/j.cplett.2017.01.071.

[8] I. Yamanaka, T. Onisawa, T. Hashimoto, T. Murayama, A fuel-cell reactor for the direct synthesis of hydrogen peroxide alkaline solutions from H2 and O2, ChemSusChem. 4 (2011) 494–501. doi:10.1002/cssc.201000263.

[9] I. Yamanaka, T. Onizawa, S. Takenaka, K. Otsuka, Direct and continuous production of hydrogen peroxide with 93% selectivity using a fuel-cell system, Angew. Chemie - Int. Ed. 42 (2003) 3653–3655. doi:10.1002/anie.200351343.

[10] J.K. Edwards, B. Solsona, E.N. N, A.F. Carley, A. a Herzing, C.J. Kiely, G.J. Hutchings, Switching Off Hydrogen Peroxide Hydrogenation in the Direct Synthesis Process, Science (80-.). 323 (2009) 1037–1041. doi:10.1126/science.1168980.

[11] E. Brillas, F. Alcaide, P.L. Cabot, A small-scale flow alkaline fuel cell for on-site production of hydrogen peroxide, Electrochim. Acta. 48 (2002) 331–340. doi:10.1016/S0013-4686(02)00665-5.

[12] J.S. Jirkovský, I. Panas, E. Ahlberg, M. Halasa, S. Romani, D.J. Schiffrin, Single atom hot-spots at Au-Pd nanoalloys for electrocatalytic H 2O 2 production, J. Am. Chem. Soc. 133 (2011) 19432–19441. doi:10.1021/ja206477z.

[13] S. Siahrostami, A. Verdaguer-Casadevall, M. Karamad, D. Deiana, P. Malacrida, B. Wickman, M. Escudero-Escribano, E.A. Paoli, R. Frydendal, T.W. Hansen, I. Chorkendorff, I.E.L. Stephens, J. Rossmeisl, Enabling direct H2O2 production through rational electrocatalyst design, Nat. Mater. 12 (2013) 1137–1143. doi:10.1038/nmat3795.

[14] E. Lobyntseva, T. Kallio, N. Alexeyeva, K. Tammeveski, K. Kontturi, Electrochemical synthesis of hydrogen peroxide: Rotating disk electrode and fuel cell studies, Electrochim. Acta. 52 (2007) 7262–7269. doi:10.1016/j.electacta.2007.05.076.

[15] T.P. Fellinger, F. Hasché, P. Strasser, M. Antonietti, Mesoporous nitrogen-doped carbon for the electrocatalytic synthesis of hydrogen peroxide, J. Am. Chem. Soc. 134 (2012) 4072–4075. doi:10.1021/ja300038p.

[16] C.H. Choi, H.C. Kwon, S. Yook, H. Shin, H. Kim, M. Choi, Hydrogen peroxide synthesis via enhanced two-electron oxygen reduction pathway on carbon-coated pt surface, J. Phys. Chem. C. 118 (2014) 30063–30070. doi:10.1021/jp5113894.

[17] E. Pizzutilo, S.J. Freakley, S. Geiger, C. Baldizzone, A. Mingers, G.J. Hutchings, K.J.J. Mayrhofer, S. Cherevko, Addressing stability challenges of using bimetallic electrocatalysts: the case of gold–palladium nanoalloys, Catal. Sci. Technol. 7 (2017) 1848–1856. doi:10.1039/C7CY00291B.

[18] E. Pizzutilo, S.J. Freakley, S. Cherevko, S. Venkatesan, G.J. Hutchings, C.H. Liebscher, G. Dehm, K.J.J. Mayrhofer, Gold-Palladium Bimetallic Catalyst Stability: Consequences for Hydrogen Peroxide Selectivity, ACS Catal. 7 (2017) 5699–5705. doi:10.1021/acscatal.7b01447.

[19] F. Jaouen, E. Proietti, M. Lefèvre, R. Chenitz, J.-P. Dodelet, G. Wu, H.T. Chung, C.M. Johnston, P. Zelenay, Recent advances in non-precious metal catalysis for oxygen-reduction reaction in polymer electrolyte fuelcells, Energy Environ. Sci. 4 (2011) 114–130. doi:10.1039/C0EE00011F.

[20] S.B. Shin, D. Chadwick, Kinetics of Heterogeneous Catalytic Epoxidation of Propene with Hydrogen Peroxide over Titanium Silicalite (TS-1), Ind. Eng. Chem. Res. 49 (2010) 8125–8134. doi:10.1021/ie100083u.

[21] A. Damjanovic, M.A. Genshaw, J.O. Bockris, The Role of Hydrogen Peroxide in Oxygen Reduction at Platinum in H_2SO_4 Solution, J. Electrochem. Soc. . 114 (1967) 466–472. doi:10.1149/1.2426629.

[22] N.M. Marković, H.A. Gasteiger, B.N. Grgur, P.N. Ross, Oxygen reduction reaction on Pt(111): effects of bromide, J. Electroanal. Chem. 467 (1999) 157–163. doi:https://doi.org/10.1016/S0022-0728(99)00020-0.

[23] T.J. Schmidt, U.A. Paulus, H.A. Gasteiger, R.J. Behm, The oxygen reduction reaction on a

Pt/carbon fuel cell catalyst in the presence of chloride anions, J. Electroanal. Chem. 508 (2001) 41–47. doi:https://doi.org/10.1016/S0022-0728(01)00499-5.

[24] I. Katsounaros, W.B. Schneider, J.C. Meier, U. Benedikt, P.U. Biedermann, A.A. Auer, K.J.J. Mayrhofer, Hydrogen peroxide electrochemistry on platinum: towards understanding the oxygen reduction reaction mechanism, Phys. Chem. Chem. Phys. 14 (2012) 7384. doi:10.1039/c2cp40616k.

[25] I. Katsounaros, W.B. Schneider, J.C. Meier, U. Benedikt, P.U. Biedermann, A. Cuesta, A.A. Auer, K.J.J. Mayrhofer, The impact of spectator species on the interaction of H2O 2 with platinum-implications for the oxygen reduction reaction pathways, Phys. Chem. Chem. Phys. 15 (2013) 8058–8068. doi:10.1039/c3cp50649e.

[26] M. Arenz, T.J. Schmidt, K. Wandelt, P.N. Ross, N.M. Markovic, The Oxygen Reduction Reaction on Thin Palladium Films Supported on a Pt(111) Electrode, J. Phys. Chem. B. 107 (2003) 9813–9819. doi:10.1021/jp034789m.

[27] V. Climent, N.M. Marković, P.N. Ross, Kinetics of Oxygen Reduction on an Epitaxial Film of Palladium on Pt(111) † , ‡, J. Phys. Chem. B. 104 (2000) 3116–3120. doi:10.1021/jp993480t.

[28] K. Ke, T. Hatanaka, Y. Morimoto, Reconsideration of the quantitative characterization of the reaction intermediate on electrocatalysts by a rotating ring-disk electrode: The intrinsic yield of H2O2 on Pt/C, Electrochim. Acta. 56 (2011) 2098–2104. doi:10.1016/j.electacta.2010.11.086.

[29] M. Inaba, H. Yamada, J. Tokunaga, A. Tasaka, Effect of Agglomeration of Pt/C Catalyst on Hydrogen Peroxide Formation, Electrochem. Solid-State Lett. 7 (2004) A474. doi:10.1149/1.1814595.

[30] A. Bonakdarpour, T.R. Dahn, R.T. Atanasoski, M.K. Debe, J.R. Dahn, H2O2 Release during Oxygen Reduction Reaction on Pt Nanoparticles, Electrochem. Solid-State Lett. 11 (2008) B208. doi:10.1149/1.2978090.

[31] I. Katsounaros, J.C. Meier, K.J.J. Mayrhofer, The impact of chloride ions and the catalyst loading on the reduction of H2O2 on high-surface-area platinum catalysts, Electrochim. Acta. 110 (2013) 790–795. doi:10.1016/j.electacta.2013.03.156.

[32] G. V. Fortunato, E. Pizzutilo, A.M. Mingers, O. Kasian, S. Cherevko, E.S.F. Cardoso, K.J.J. Mayrhofer, G. Maia, M. Ledendecker, Impact of Palladium Loading and Interparticle

Distance on the Selectivity for the Oxygen Reduction Reaction toward Hydrogen Peroxide, J. Phys. Chem. C. 122 (2018) 15878–15885. doi:10.1021/acs.jpcc.8b04262.

[33] F. de Lima, G. Maia, Oxidized/reduced graphene nanoribbons facilitate charge transfer to the Fe(CN) 6 3− /Fe(CN) 6 4− redox couple and towards oxygen reduction, Nanoscale. 7 (2015) 6193–6207. doi:10.1039/C5NR01123J.

[34] E.I. Khrushcheva, M.R. Tarasevich, Electrochemical Determination of Surface Area of Metals, Russ. Chem. Rev. 47 (1978) 416–424. doi:10.1070/rc1978v047n05abeh002227.

[35] K. Jukk, N. Alexeyeva, A. Sarapuu, P. Ritslaid, J. Kozlova, V. Sammelselg, K. Tammeveski, Electroreduction of oxygen on sputter-deposited Pd nanolayers on multi-walled carbon nanotubes, Int. J. Hydrogen Energy. 38 (2013) 3614–3620. doi:10.1016/j.ijhydene.2013.01.062.

[36] A. Zalineeva, S. Baranton, C. Coutanceau, Bi-modified palladium nanocubes for glycerol electrooxidation, Electrochem. Commun. 34 (2013) 335–338. doi:10.1016/j.elecom.2013.07.022.

[37] I.M. Tidswell, N.M. Markovic, P.N. Ross, Potential dependent surface structure of the Pt(1 1 1) electrolyte interface, J. Electroanal. Chem. 376 (1994) 119–126. doi:https://doi.org/10.1016/0022-0728(94)03553-9.

[38] C.A. Lucas, N.M. Marković, P.N. Ross, Surface Structure and Relaxation at the Pt(110)/Electrolyte Interface, Phys. Rev. Lett. 77 (1996) 4922–4925. doi:10.1103/PhysRevLett.77.4922.

[39] N.M. Marković, B.N. Grgur, P.N. Ross, Temperature-Dependent Hydrogen Electrochemistry on Platinum Low-Index Single-Crystal Surfaces in Acid Solutions, J. Phys. Chem. B. 101 (1997) 5405–5413. doi:10.1021/jp970930d.

[40] M.W. Breiter, Dissolution and adsorption of hydrogen at smooth Pd wires at potentials of the alpha phase. Influence of electrolyte, J. Electroanal. Chem. Interfacial Electrochem. 90 (1978) 425–430. doi:https://doi.org/10.1016/S0022-0728(78)80077-1.

[41] M. Grdeń, M. Łukaszewski, G. Jerkiewicz, A. Czerwiński, Electrochemical behaviour of palladium electrode: Oxidation, electrodissolution and ionic adsorption, Electrochim. Acta. 53 (2008) 7583–7598. doi:10.1016/j.electacta.2008.05.046.

[42] M.I. Kulezneva, N.A. Balashova, Adsorption of ions on Pd. Pt. 2. Dependence of the adsorption of bromine and iodine ions on the potential and concentration in acidified

solutions, Elektrokhimiya. 7 (1971) 448–452.

[43] M. Arenz, Model electrodes for electrocatalysis: Ultrathin palladium films on Pt (111), Rheinischen Friedrich-Wilhelms-Universität Bonn, 2002.

[44] U.A. Paulus, T.J. Schmidt, H.A. Gasteiger, R.J. Behm, Oxygen reduction on a high-surface area Pt/Vulcan carbon catalyst: a thin-film rotating ring-disk electrode study, J. Electroanal. Chem. 495 (2001) 134–145. doi:10.1016/S0022-0728(00)00407-1.

[45] O. Antoine, R. Durand, RRDE study of oxygen reduction on Pt nanoparticles inside Nafion®: H2O2 production in PEMFC cathode conditions, J. Appl. Electrochem. 30 (2000) 839–844. doi:10.1023/A:1003999818560.

[46] D.A. Crole, S.J. Freakley, J.K. Edwards, G.J. Hutchings, Direct synthesis of hydrogen peroxide in water at ambient temperature, Proc. R. Soc. A Math. Phys. Eng. Sci. 472 (2016). doi:10.1098/rspa.2016.0156.

[47] D.W. Flaherty, Direct Synthesis of H2O2 from H2 and O2 on Pd Catalysts: Current Understanding, Outstanding Questions, and Research Needs, ACS Catal. 8 (2018) 1520–1527. doi:10.1021/acscatal.7b04107.

[48] V.R. Choudhary, C. Samanta, Role of chloride or bromide anions and protons for promoting the selective oxidation of H2 by O2 to H2O2 over supported Pd catalysts in an aqueous medium, J. Catal. 238 (2006) 28–38. doi:10.1016/j.jcat.2005.11.024.

[49] C. Samanta, V.R. Choudhary, Direct synthesis of H2O2 from H2 and O2 and decomposition/hydrogenation of H2O2 in an aqueous acidic medium over halide-modified Pd/Al2O3 catalysts, Appl. Catal. A Gen. 330 (2007) 23–32. doi:10.1016/j.apcata.2007.06.030.

[50] V. Choudhary, P. Jana, Synergetic effect of two halogen promoters present in acidic reaction medium or catalyst on the H2O2 formation (in H2-to-H2O2 oxidation) and destruction over Pd/C (or Al2O3) catalyst, J. Catal. 246 (2007) 434–439. doi:10.1016/j.jcat.2006.12.012.

[51] G. Polymeros, C. Baldizzone, S. Geiger, J.P. Grote, J. Knossalla, S. Mezzavilla, G.P. Keeley, S. Cherevko, A.R. Zeradjanin, F. Schüth, K.J.J. Mayrhofer, High temperature stability study of carbon supported high surface area catalysts—Expanding the boundaries of ex-situ diagnostics, Electrochim. Acta. 211 (2016) 744–753. doi:https://doi.org/10.1016/j.electacta.2016.06.105.

[52] E. Pizzutilo, S. Geiger, J.-P. Grote, A. Mingers, K.J.J. Mayrhofer, M. Arenz, S. Cherevko,

On the Need of Improved Accelerated Degradation Protocols (ADPs): Examination of Platinum Dissolution and Carbon Corrosion in Half-Cell Tests, J. Electrochem. Soc. . 163 (2016) F1510–F1514. doi:10.1149/2.0731614jes.

[53] S. Mezzavilla, S. Cherevko, C. Baldizzone, E. Pizzutilo, G. Polymeros, K.J.J. Mayrhofer, Experimental Methodologies to Understand Degradation of Nanostructured Electrocatalysts for PEM Fuel Cells: Advances and Opportunities, ChemElectroChem. 3 (2016) 1524–1536. doi:10.1002/celc.201600170.

[54] J.G. Vos, M.T.M. Koper, Measurement of competition between oxygen evolution and chlorine evolution using rotating ring-disk electrode voltammetry, J. Electroanal. Chem. 819 (2018) 260–268. doi:10.1016/j.jelechem.2017.10.058.

[55] R. Gusmão, Z. Sofer, M. Nováček, M. Pumera, Contrasts between Mild and Harsh Oxidation of Carbon Nanotubes in terms of their Properties and Electrochemical Performance, ChemElectroChem. 3 (2016) 1713–1719. doi:10.1002/celc.201600082.

[56] S. Kabir, A. Serov, A. Zadick, K. Artyushkova, P. Atanassov, Palladium Nanoparticles Supported on Three-Dimensional Graphene Nanosheets: Superior Cathode Electrocatalysts, ChemElectroChem. 3 (2016) 1655–1666. doi:10.1002/celc.201600245.

[57] E. Pizzutilo, S. Geiger, S.J. Freakley, A. Mingers, S. Cherevko, G.J. Hutchings, K.J.J. Mayrhofer, Palladium electrodissolution from model surfaces and nanoparticles, Electrochim. Acta. 229 (2017) 467–477. doi:10.1016/j.electacta.2017.01.127.

Graphical abstract